Functionally additive fixed positive and negative charges in the CFTR channel pore control anion binding and conductance

Received for publication, October 26, 2021, and in revised form, January 14, 2022 Published, Papers in Press, January 29, 2022,
https://doi.org/10.1016/j.jbc.2022.101659

Paul Linsdell*, Christina L. Irving, and Elizabeth A. Cowley
From the Department of Physiology & Biophysics, Dalhousie University, Halifax, Nova Scotia, Canada

Edited by Mike Shipston

Ion channels use charged amino-acid residues to attract oppositely charged permeant ions into the channel pore. In the cystic fibrosis transmembrane conductance regulator (CFTR) Cl^- channel, a number of arginine and lysine residues have been shown to be important for Cl^- permeation. Among these, two in close proximity in the pore—Lys^{95} and Arg^{134}—are indispensable for anion binding and high Cl^- conductance, suggesting that high positive charge density is required for pore function. Here we used mutagenesis and functional characterization to show that a nearby pore-lining negatively charged residue (Glu^{92}) plays a functionally additive role with these two positive charges. While neutralization of this negative charge had little effect on anion binding or Cl^- conductance, such neutralization was able to reverse the detrimental effects of removing the positive charge at either Lys^{95} or Arg^{134}, as well as the similar effects of introducing a negative charge at a neighboring residue (Ser^{1141}). Furthermore, neutralization of Glu^{92} greatly increased the susceptibility of the channel to blockage by divalent $S_2O_3^{2-}$ anions, mimicking the effect of introducing additional positive charge in this region; this effect was reversed by concurrent neutralization of either Lys^{95} or Arg^{134}. Across a panel of mutant channels that introduced or removed fixed charges at these four positions, we found that many pore properties are dependent on the overall charge or charge density. We propose that the CFTR pore uses a combination of positively and negatively charged residues to optimize the anion binding and Cl^- conductance properties of the channel.

Cystic fibrosis (CF) is caused by loss-of-function mutations in the cystic fibrosis transmembrane conductance regulator (CFTR), an epithelial cell Cl^- channel (1). Both functional (1, 2) and structural data (3, 4) have highlighted the important role of positively charged amino acid side chains in Cl^- permeation through the channel pore (Fig. 1). Several positively charged side chains are clustered around the internal and external mouths of the pore (3, 4) (Fig. 1). Neutralization of these positive charges reduces Cl^- conductance (5–9), most likely because these charges are important in attracting Cl^- to the pore (2, 9). Within the pore, an uncharged, narrow extracellular region forms both the selectivity filter and the channel gate and also plays a major role in determining overall Cl^- conductance (1, 2). This narrow region is connected to the cytoplasm *via* a relatively wide inner vestibule (Fig. 1) that is thought to be an important region for anion binding (1, 2). Within this inner vestibule, two positively charged side chains —Lys^{95} and Arg^{134}—have been shown to play particularly important, analogous roles in Cl^- conductance and anion binding (10, 11). Thus, neutralization of either of these positive charges results in a drastic (≥90%) reduction in Cl^- conductance (11–13). Removal of either of these charges also greatly reduces the binding affinity of both permeant anions (10–12) and large anions that act as open-channel blockers by lodging within the inner vestibule (11, 13, 14). Additionally, neutralization of either practically abolishes the normal permeant anion conductance selectivity sequence, in which lyotropic permeant anions (such as SCN^-) normally show a lower conductance than Cl^- (11, 15). This suggests that permeant anion binding close to these positive charges is a major determinant of conductance selectivity (11, 15). Molecular dynamics simulations also suggest that both Lys^{95} and Arg^{134} contribute to an important Cl^- binding site in the inner vestibule (16).

In spite of their important functional roles, the absolute positioning of the positive charges at these two sites, in the first (Lys^{95}) and second (Arg^{134}) of CFTR's 12 transmembrane α-helices (TMs), does not appear essential. Thus, mutagenesis can be used to "transplant" either of these positive charges to other nearby sites in the inner vestibule, such as Ile^{344} and Val^{345} (TM6) or Ser^{1141} (TM12) (11, 13, 17). The observation that such charge-transplanted channels show well-restored, wild-type-like Cl^- conductance, anion binding, and conductance selectivity properties (10, 11, 13, 17, 18) suggests that these other sites are permissive hosts for these functionally important charges. However, introduction of additional, ectopic positive charge (by mutagenesis of these permissive sites in the presence of endogenous charges at both Lys^{95} and Arg^{134}) does not appear drastically to alter anion conductance or anion-binding properties (10, 13, 17). Instead, the major functional effect of introducing extra positive charge in the inner vestibule appears to be a drastic increase in the binding

* For correspondence: Paul Linsdell, paul.linsdell@dal.ca.

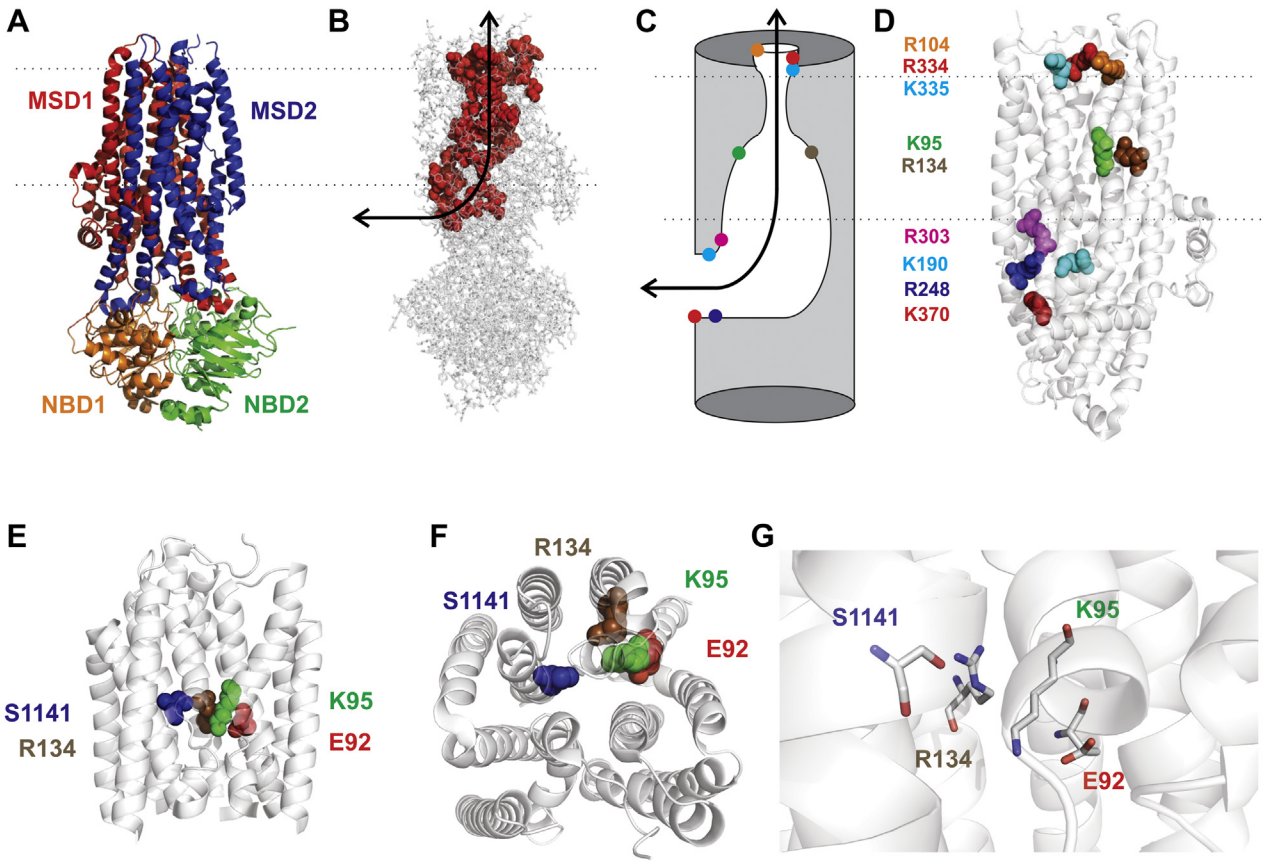

Figure 1. Structure of the CFTR pore region. *A*, atomic structure of human CFTR in a phosphorylated, ATP-bound state (4). *Different colors* represent different domains, the two membrane-spanning domains (MSDs) and two cytoplasmic nucleotide binding domains (NBDs). The cytoplasmic regulatory domain is absent from this structure. *B*, location of putative pore-lining side-chains (*red* space-filling models) in the same structure (11), and proposed pathway for Cl^- permeation (*black arrow*) (34). *C*, cartoon model of the pore, based on recent reviews (2, 34) and illustrating the location of pore-lining positively charged side chains in the outer vestibule (Arg^{104}, Arg^{334}, Lys^{335}), inner vestibule (Lys^{95}, Arg^{134}) and cytoplasmic portal region (Lys^{190}, Arg^{248}, Arg^{303}, Lys^{370}). The outer and inner vestibules are connected by a narrow, uncharged region (selectivity filter). *D*, location of these positively charged side-chains within the MSDs; same structure as in (*A*), with the NBDs removed. Space-filling models of side chains are the same colors as in (*C*). *Dotted lines* indicate the approximate extent of the membrane in (*A–D*). *E* and *F*, location of amino acids mutated in the present study, within close-up views of the TMs viewed from the side (*E*) or from the extracellular space (*F*). *G*, spatial proximity of these four side-chains in a closer view of the same structure. Distances from Glu^{92} (β carbon-β carbon distance) are: Lys^{95}, 5.9 Å; Arg^{134}, 15.3 Å; Ser^{1141}, 8.7 Å (other distances given in (11)). CFTR, cystic fibrosis transmembrane conductance regulator.

affinity of divalent anions (10, 13, 17, 19) (in spite of little change in binding affinity of monovalent anions, including Cl^- itself (10)). This finding has been used to suggest that the number (or density) of fixed positive charges in the inner vestibule of the wild-type CFTR pore is well optimized to select for monovalent over divalent anions (19).

One puzzle is: why should two fixed positive charges in this region result in a monovalent-selective anion channel, whereas adding a third favors binding of divalent anions? The present work investigates the role of a nearby pore-lining *negative* charge—that of Glu^{92} in TM1 (Fig. 1)—in acting in an additive way with the positive charges of Lys^{95} and Arg^{134} to determine CFTR anion binding and conductance.

Results

Expression of Glu^{92}-mutant CFTR

Previous work has indicated difficulty in obtaining functional expression of Glu^{92}-mutant forms of CFTR in mammalian cells (20, 21). Western blot analysis showed that several different Glu^{92} mutants were able to generate mature, complex glycosylated (Band C) protein when expressed in baby hamster kidney (BHK) cells (Fig. 2), implying that at least some protein should be trafficked to the cell membrane. However, the relative abundance of this mature protein form appeared sensitive to the charge of the side chain at position 92: negative charge (wild-type, E92D) produced mostly mature protein, neutral charge (E92N, E92Q) significantly less, and positive charge (E92K, E92R) almost no detectable Band C protein (Fig. 2). One deviation from this apparent pattern was E92T, which also produced almost no Band C protein (Fig. 2). To test for possible interactions with nearby native positive charges, we also introduced E92K into backgrounds where these charges were neutralized (K95Q, R134Q) or reversed (K95E, R134E). Of these, only K95E was able to reverse the apparent effects of E92K on protein processing, leading to the appearance of significant amounts of Band C protein (Fig. 2). Mutation of Lys^{95} alone had little apparent effect on CFTR protein

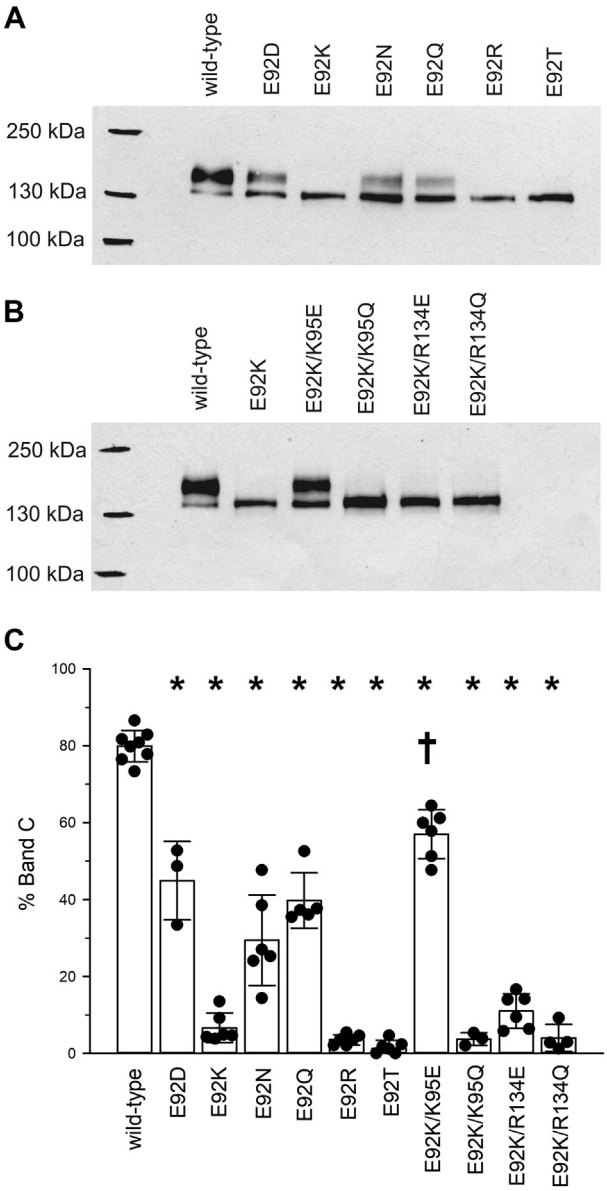

Figure 2. Protein expression of different CFTR variants expressed in BHK cells. *A* and *B*, representative Western blots for CFTR using protein from BHK cells transfected with the named CFTR variants. *C*, abundance of Band C protein (as a percentage of total) as determined by densitometric analysis. Tests of significance were carried out using one-way ANOVA with Bonferroni correction. *Asterisks* indicate a significant difference from wild-type ($p < 0.001$), while for double-mutant proteins *daggers* indicate a significant difference from E92K ($p < 0.001$). Each point represents data from an independent transfection. Bars represent mean ± SD from $n = 8$ (wild-type), 3 (E92D), 6 (E92K), 6 (E92N), 5 (E92Q), 6 (E92R), 6 (E92T), 6 (E92K/K95E), 3 (E92K/K95Q), 6 (E92K/R134E), and 4 (E92K/R134Q) independent transfections. CFTR, cystic fibrosis transmembrane conductance regulator.

processing (see Supporting information). Recently, we showed that R134E and R134Q also had only moderate effects on CFTR protein processing under identical conditions (11).

Negative charge in the pore moderates block by divalent anions

A characteristic effect of the introduction of ectopic fixed positive charge in the inner vestibule of the pore is a drastic strengthening of block by intracellular divalent anions (10, 17–19, 22). Similar effects were observed following removal of the negative charge at position 92, as illustrated by the effect of different mutations on block by $S_2O_3^{2-}$ (Fig. 3). Thus, in E92N and E92Q (E1371Q background—see Experimental procedures)—but not in charge-conservative E92D/E1371Q—this divalent anion caused a strong, highly voltage-dependent block that is practically absent in control E1371Q-CFTR channels (Fig. 3). At the most negative voltages studied, $S_2O_3^{2-}$ blocked E92N/E1371Q and E92Q/E1371Q with K_Ds of ∼1 mM (Fig. 3, *C–E*), more than an order of magnitude lower than for E1371Q (Fig. 3*B*). A similar strong blocking effect was also observed in E92T/E1371Q (Fig. 4*B*), although this mutant gave only very small macroscopic currents that precluded detailed analysis. E92K/E1371Q and E92R/E1371Q expression produced no noticeable current under these conditions, consistent with the Western blot results (Fig. 2).

Strong block by $S_2O_3^{2-}$ suggests that the functional effect of removing a fixed negative charge in the pore may be similar to that of introducing a fixed positive charge (19). To test this, mutagenesis was used to alter the fixed charge at two sites simultaneously. The strong blocking effect of $S_2O_3^{2-}$ on E92Q/E1371Q was effectively reversed by mutations that either remove a positive charge (K95Q, R134Q) or introduce an ectopic negative charge at a nearby site (S1141E) (Fig. 4). These results suggest that the balance between positive and negative charges in this part of the pore determines the binding affinity for intracellular divalent anions. In support of this idea, the double pore-mutant E92K/K95E (E1371Q background)—which effectively reverses the positions of negatively and positively charged side chains in TM1—showed similar $S_2O_3^{2-}$ block as E1371Q (Fig. 4*B*). E92K/K95Q/E1371Q, E92K/R134E/E1371Q, and E92K/R134Q/E1371Q failed to generate any current under these conditions, again consistent with Western blot results (Fig. 2).

Positive and negative charges control unitary conductance

The positive charges at Lys^{95} and Arg^{134} play key roles in maximizing unitary conductance in CFTR (see the start of the text); mutations that remove either of these positive charges reduce conductance by ≥90% (11–13) (Fig. 5, *A*, *B* and *E*). In contrast, mutagenesis of Glu^{92} (E92D, E92N, E92Q, E92T) had no significant effect on conductance (Fig. 5, *A* and *E*). However, neutralization of this negative charge (in E92Q) was able to partially reverse the effects of K95Q and R134Q on conductance (Fig. 5, *A*, *B*, *D* and *E*). Whereas the conductance of K95Q was only 9.8 ± 0.5% ($n = 5$) of wild-type, this was increased to 87 ± 2% ($n = 5$) of wild-type in E92Q/K95Q ($p < 0.001$) (Fig. 5, *A*, *B*, *D* and *E*). The conductance of R134Q is too low to be quantified using single-channel recording (11); however, E92Q/R134Q channels had a conductance 52 ± 2% ($n = 4$) of wild-type (Fig. 5, *D* and *E*). Introduction of an extra negative charge (in S1141E) was highly disruptive to channel function, leading to a reduction in conductance to below the limits of resolution, similar to the effects of removing the

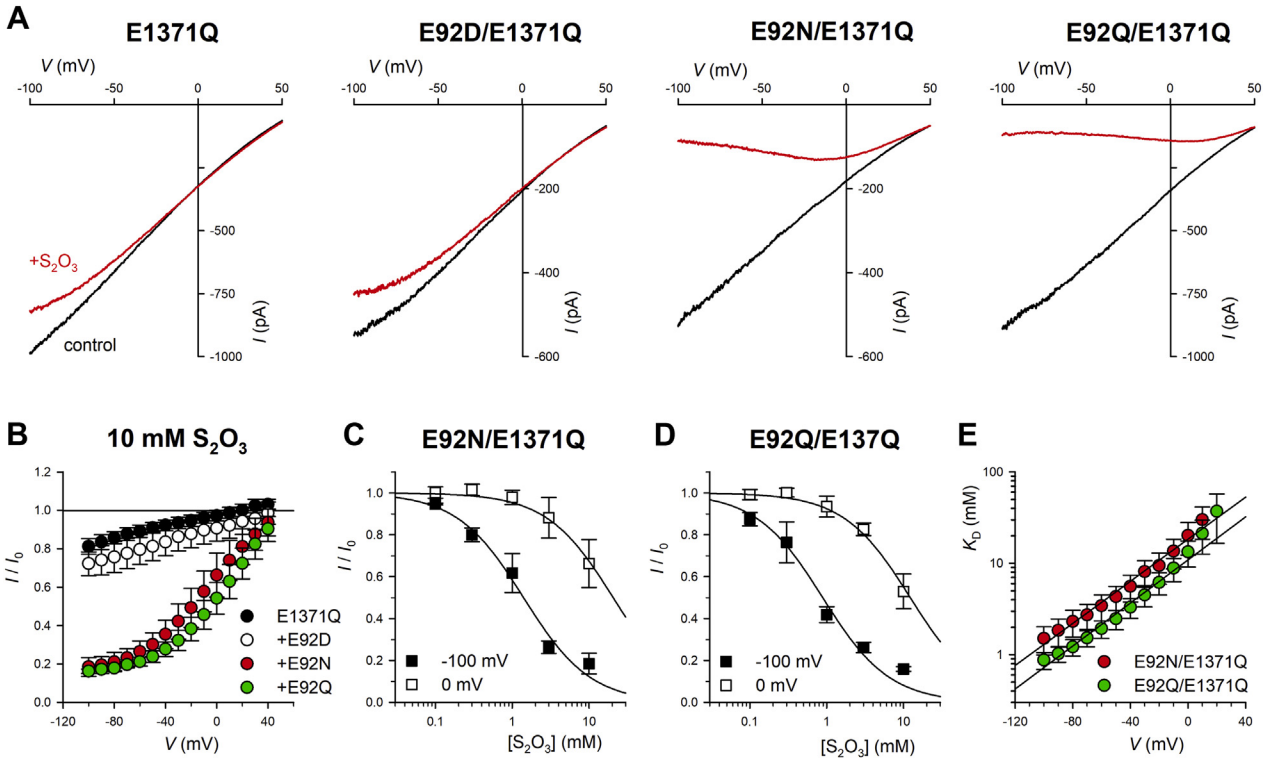

Figure 3. Strong block of Glu^{92}-mutant CFTR by intracellular $S_2O_3^{2-}$. *A*, example *I-V* relationships for E1371Q and Glu^{92}-mutant CFTR (E1371Q background) recorded before (*black lines*) and after addition of 10 mM $S_2O_3^{2-}$ to the intracellular solution (*red lines*). *B*, direct comparison of the voltage-dependent effects of 10 mM $S_2O_3^{2-}$ on these channel variants (E1371Q background). Data points represent mean ± SD from n = 5 (E1371Q), 4 (E92D/E1371Q), 4 (E92N/E1371Q) and 5 (E92Q/E1371Q) patches. *C* and *D*, concentration-dependent effects of $S_2O_3^{2-}$ on E92N/E1371Q (*C*) and E92Q/E1371Q (*D*), quantified at membrane potentials of −100 mV (■) and 0 mV (❑). Data points represent mean ± SD from four patches in each condition and have been fitted as described under "Experimental procedures" (Equation 1), giving K_Ds of 1.41 mM (−100 mV) and 20.6 mM (0 mV) for E92N/E1371Q, and 0.89 mM (−100 mV) and 12.2 mM (0 mV) for E92Q/E1371Q. *E*, mean K_D values (±SD) for E92N/E1371Q (●) (n = 6) and E92Q/E1371Q (○) (n = 8) obtained from such fits as a function of membrane potential. The slope of this relationship at negative voltages allows quantification of blocker effective valence ($z\delta$) as described under "Experimental procedures" (Equation 2), giving mean $z\delta$ values of −0.72 ± 0.16 (n = 6) for E92N/E1371Q and −0.83 ± 0.10 (n = 8) for E92Q/E1371Q. These $z\delta$ values are somewhat lower than was recently reported for I344K/E1371Q and S1141K/E1371Q under identical conditions (19). CFTR, cystic fibrosis transmembrane conductance regulator.

positive charges of Lys^{95} or Arg^{134} (Fig. 5*E*). This dramatic reduction in conductance was partly reversed by the E92Q mutation (*i.e.*, in E92Q/S1141E) that effectively "moves" the negative charge from TM1 (Glu^{92}) to TM12 (Ser^{1141}), although the conductance of E92Q/S1141E (26 ± 2% (n = 6) of wild-type) was noticeably lower than either E92Q/K95Q or E92Q/R134Q (see above) (Fig. 5, *D* and *E*). These results are consistent with the overall charge at positions 92, 95, 134, and 1141 controlling conductance (Fig. 5*D*). Consistent with this idea, the charge-switching E92K/K95E mutant showed retained channel function, with a conductance 60 ± 1% (n = 7) of wild-type (Fig. 5, *A*, *C* and *E*).

Positive and negative charges control anion binding

The positive charges of Lys^{95} and Arg^{134} are also important for anion binding in the inner vestibule, and neutralization of these charges affects the binding affinity of permeant and blocking anions (see the start of the text). Block of Cl^- permeation by intracellular permeant $Au(CN)_2^-$ ions was slightly weakened in E92Q-mutant channels (mean K_D (at −40 mV) increased from 40.0 ± 8.5 μM (n = 8) in E1371Q to 123 ± 32 μM (n = 6) in E92Q/E1371Q) (Fig. 6, *A*–*C*), consistent with the moderate effects of mutations that increase the number of positive charges (Q98K, I344K, V345K, S1141K (10)). Addition of negative charge (in S1141E/E1371Q) drastically weakened $Au(CN)_2^-$ block (mean K_D (−40 mV) 5990 ± 870 μM (n = 4)) (Fig. 6, *A*–*C*), to an even greater extent than removal of endogenous positive charge (K95Q/E1371Q, R134Q/E1371Q; Fig. 6, *D* and *E*; (10, 11)). This apparent loss of $Au(CN)_2^-$ binding in S1141E/E1371Q was mostly (>90%) reversed in E92Q/S1141E/E1371Q (mean K_D (−40 mV) 359 ± 105 μM (n = 6)) (Fig. 6, *A*–*D*). The E92Q mutation was also able to reverse the effects of K95Q and R134Q by >90% (Fig. 6*D*), indicating that a balance between fixed positive and negative charges determines $Au(CN)_2^-$ binding affinity. Consistent with this, the charge-switching E92K/K95E mutant (E1371Q background) showed retained $Au(CN)_2^-$ binding (mean K_D (−40 mV) 235 ± 70 μM (n = 4)) (Fig. 6*E*).

Block of Cl^- permeation by intracellular 5-nitro-2-(3-phenylpropylamino)benzoic acid (NPPB) showed a similar pattern. Thus, E92Q itself (E1371Q background) did not significantly alter the blocking effects of 50 μM NPPB (Fig. 7). S1141E/E1371Q showed very weak block (Fig. 7), similar to K95Q/E1371Q and R134Q/E1371Q (Fig. 7*B*) (11, 14, 17). The E92Q mutation effectively reversed the effects of K95Q,

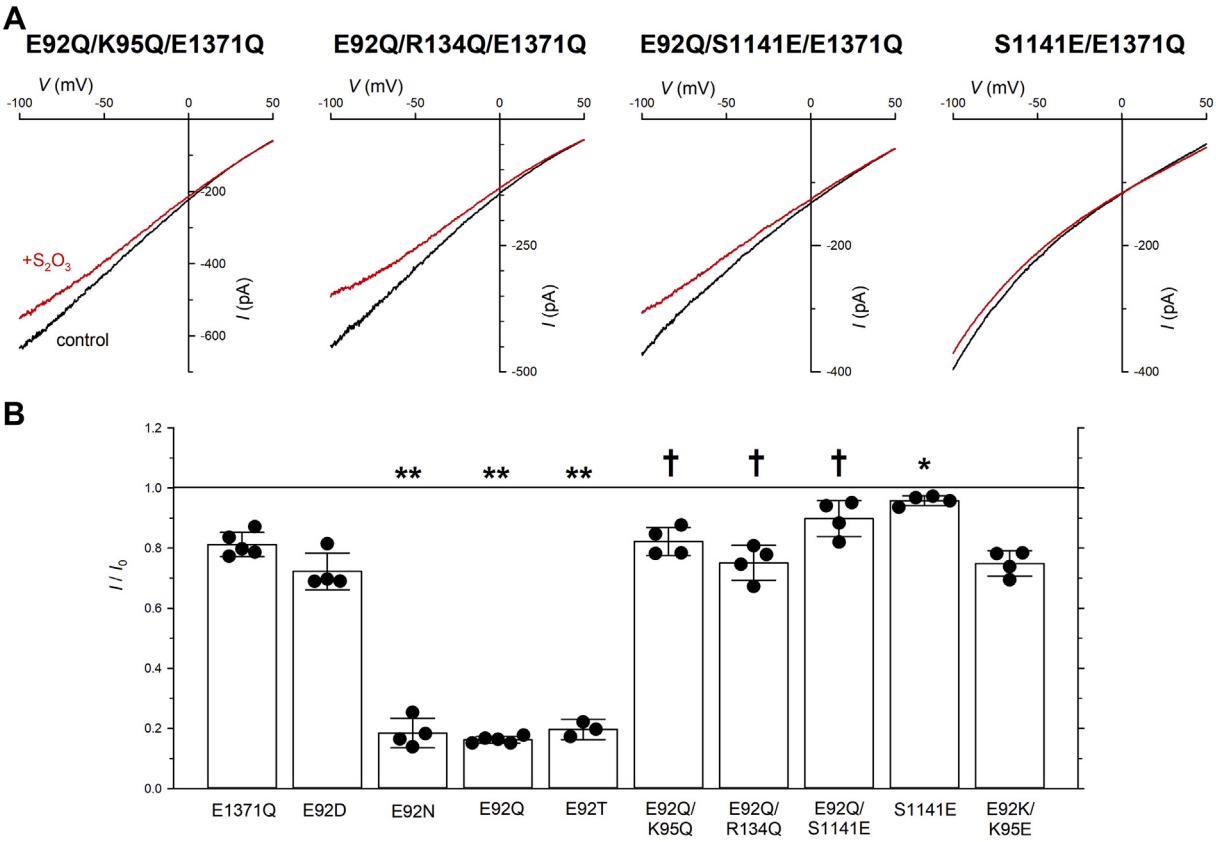

Figure 4. Reversal of strong $S_2O_3^{2-}$ block of E92Q-containing channels by second-site mutations. *A*, example *I-V* relationships for the named mutants recorded before (*black lines*) and after addition of 10 mM $S_2O_3^{2-}$ to the intracellular solution (*red lines*). *B*, effect of 10 mM $S_2O_3^{2-}$ on different channel variants (E1371Q background) at −100 mV. Tests of significance were carried out using one-way ANOVA with Bonferroni correction. *Asterisks* indicate a significant difference from E1371Q (*$p < 0.005$; **$p < 0.001$), while for E92Q-containing double pore mutant channels *daggers* indicate a significant difference from E92Q/E1371Q ($p < 0.001$). Bars represent mean ± SD from n = 5 (E1371Q), 4 (E92D/E1371Q), 4 (E92N/E1371Q), 5 (E92Q/E1371Q), 3 (E92T/E1371Q), 4 (E92Q/K95Q/E1371Q), 4 (E92Q/R134Q/E1371Q), 4 (E92Q/S1141E/E1371Q), 4 (S1141E/E1371Q), and 4 (E92K/K95E/E1371Q) patches.

R134Q, and S1141E, resulting in similar overall block as in E1371Q (Fig. 7*B*). Block of E92K/K95E/E1371Q was not significantly different from E1371Q (Fig. 7*B*).

Another apparent manifestation of anion binding in the inner vestibule is the relative conductance of different permeant anions (11, 15). Thus, mutations that remove positive charge (K95Q, R134Q) have been reported to disrupt the normal anion conductance selectivity of the channel and in particular to increase the normally very low relative conductance of lyotropic SCN^- ions (11, 15) (Fig. 8). E92Q/E1371Q showed a slightly elevated relative SCN^- conductance (G_{SCN}/G_{Cl}) compared with E1371Q (Fig. 8). In S1141E/E1371Q, SCN^- showed a considerably higher conductance than Cl^- (Fig. 8), similar to previous findings with K95Q/E1371Q and R134Q/E1371Q (11, 15) (Fig. 8). The elevated G_{SCN}/G_{Cl} seen in each of S1141E, K95Q and R134Q (E1371Q background) was effectively reversed by the comutation E92Q, restoring the wild-type pattern of low relative SCN^- conductance (Fig. 8). E92K/K95E/E1371Q also showed low G_{SCN}/G_{Cl} (Fig. 8*B*).

Discussion

Considering only the effects of single mutations, Glu^{92} does not appear to play a major role in Cl^- permeation in CFTR. Three different mutations that neutralize this negative charge—along with the charge-conserving E92D—failed to significantly alter single-channel conductance (Fig. 5), consistent with an earlier report that E92C has a similar conductance to wild-type (21). Furthermore, the charge-neutralizing E92Q mutant had only a moderate impact on permeant anion binding (assessed by $Au(CN)_2^-$ block of Cl^- permeation; Fig. 6), no effect on NPPB block (Fig. 7), and led to only a moderate weakening of Cl^-/SCN^- conductance selectivity (Fig. 8). The only hint that this negative charge might play a role in controlling pore properties is the very strong block of charge-neutralizing E92N, E92Q, and E92T (but not charge-conserving E92D) by intracellular $S_2O_3^{2-}$ ions (Fig. 3). This dramatic strengthening of $S_2O_3^{2-}$ block is highly reminiscent of the effect of mutations that introduce an ectopic positive charge within the inner vestibule of the pore, I344K and S1141K (19), and also consistent with strong open-channel block by another divalent anion, $Pt(NO_2)_4^{2-}$, when positive charge is introduced at these and other nearby pore-lining sites (10, 17–19, 22). In fact, these mutants bearing additional positive charge have also been reported to have only minor impacts on Cl^- conductance, $Au(CN)_2^-$ block, and NPPB block (10, 13, 17), as well as anion conductance selectivity (11). However, ectopic positive charge has been shown

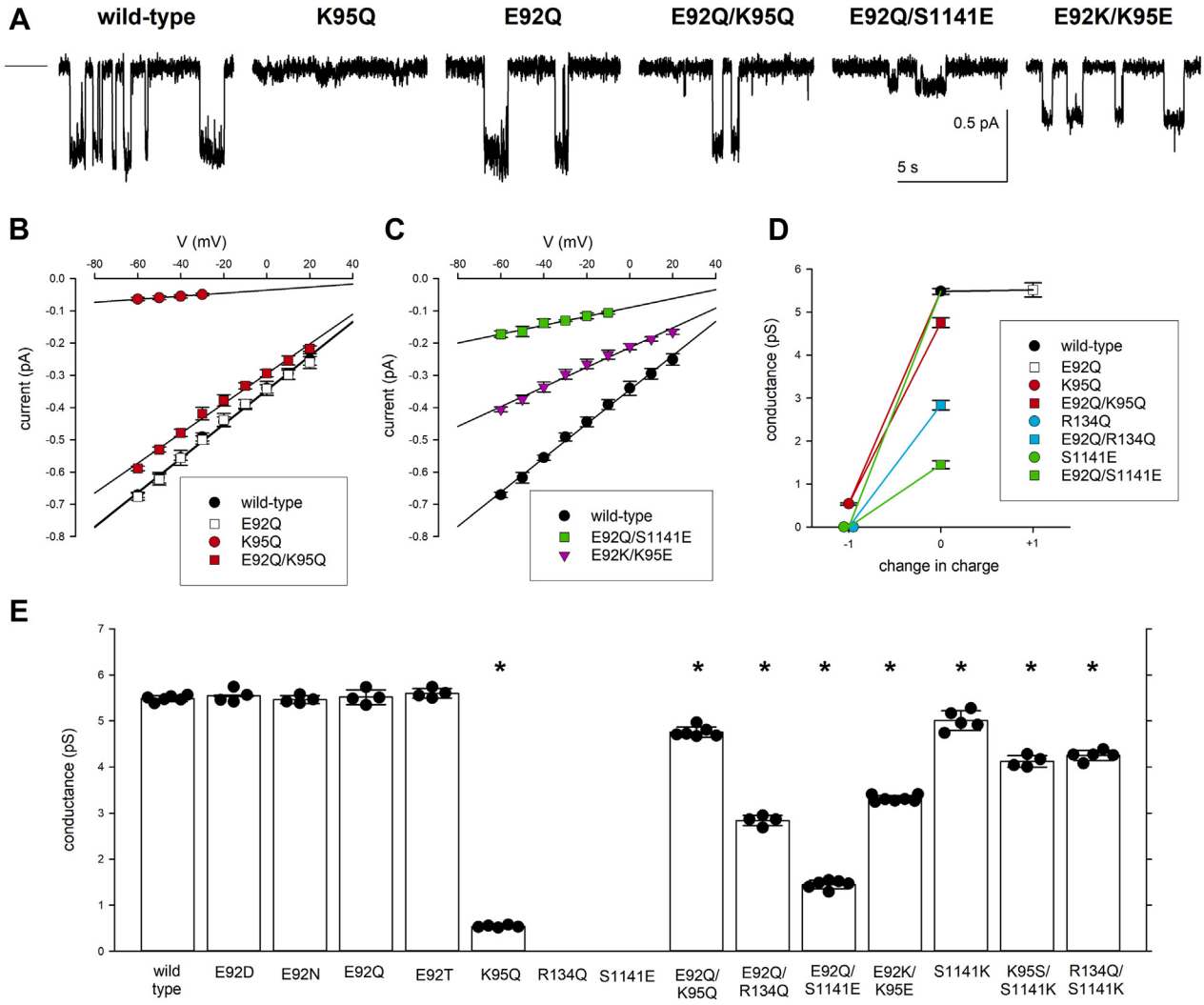

Figure 5. Single-channel conductance of different channel variants. *A*, example single channel currents carried by the named channel variants at a membrane potential of −50 mV. The closed state is indicated by the *line* to the *far left*. *B* and *C*, mean single-channel current–voltage relationships for the channel variants indicated. Data points represent mean ± SD from $n = 6$ (wild-type), 4 (E92Q), 5 (K95Q), 6 (E92Q/K95Q), 6 (E92Q/S1141E), and 5 (E92K/K95E) patches. *D* and *E*, single channel conductance measured from the slope of the current–voltage relationship from individual patches. *E*, all channel variants studied; data for S1141K and R134Q/S1141K taken from (11). The conductance of R134Q (11) and S1141E is too small to be quantified. Bars represent mean ± SD from $n = 6$ (wild-type), 4 (E92D), 4 (E92N), 4 (E92Q), 4 (E92T), 5 (K95Q), 6 (E92Q/K95Q), 4 (E92Q/R134Q), 6 (E92Q/S1141E), 7 (E92K/K95E), 5 (S1141K), 4 (K95S/S1141K), and 5 (R134Q/S1141K) patches. Tests of significance were carried out using one-way ANOVA with Bonferroni correction. *Asterisks* indicate a significant difference from wild-type ($p < 0.001$). *D*, mean effect of E92Q on conductance in different channel backgrounds. Data points represent mean ± SD from the number of patches indicated in (*E*). The *ordinate* indicates the mutagenesis-induced change in overall fixed charge in the channel pore, relative to wild-type. Whereas E92Q has no effect on conductance in a wild-type background (change in charge increased from 0 to +1), it strongly increases conductance in K95Q, R134Q and S1141E backgrounds (change in charge increased from −1 to 0) (each background indicated by a *different color*). The conductance of R134Q and S1141E is too small to be quantified.

to be able to restore the very low conductance, weak anion binding, and disrupted anion conductance selectivity associated with mutations that remove important positive charges in the inner vestibule—Lys^{95} and Arg^{134} (10, 11, 13, 17, 18). This has been interpreted as "transplantation" of functionally important positive charge from one site lining the inner vestibule to another (10, 11, 13). However, this ability to rescue the disrupted pore function of K95Q and R134Q is also shared by E92Q, leading to relatively normal wild-type (or E1371Q)-like single-channel conductance (Fig. 5), $Au(CN)_2^-$ block (Fig. 6), NPPB block (Fig. 7), and G_{SCN}/G_{Cl} (Fig. 8) in both E92Q/K95Q and E92Q/R134Q mutated channels. Conversely, K95Q and R134Q are able to reverse the effects of E92Q on $S_2O_3^{2-}$ block (Fig. 4). Thus, rather than the absolute number of positive charges lining the inner vestibule, it appears that the overall balance between fixed positive and negative charges controls anion binding in this region and thereby affects Cl^- conductance. Consistent with this, the double mutant E92K/K95E—which reverses the location of positive and negative charges—has functional properties quite similar to the wild-type/E1371Q pore (Figs. 4–8).

Anion binding in the inner vestibule is not the sole determinant of Cl^- conductance (see the start of the text). The uncharged, narrow region is thought to be a major barrier to anion conductance (10, 23), as well as the most important determinant of permeability selectivity (1, 2). Positively

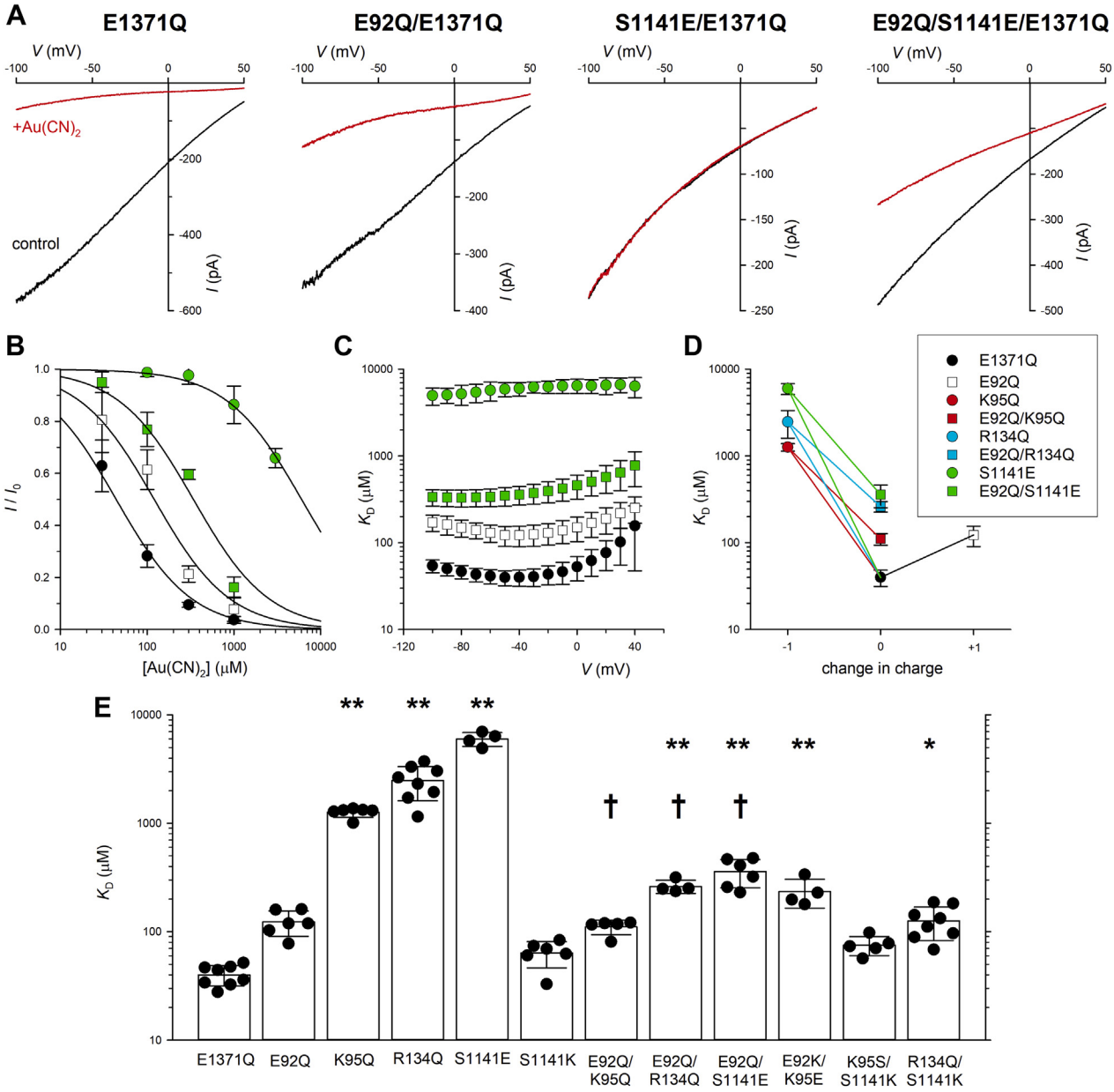

Figure 6. Block of Cl^- permeation by intracellular $Au(CN)_2^-$. *A*, example *I-V* relationships for the named variants, recorded before (*black lines*) and after addition of 300 μM $Au(CN)_2^-$ to the intracellular solution (*red lines*). *B*, mean fraction of control current remaining after addition of different concentrations of $Au(CN)_2^-$ at a membrane potential of −40 mV for these same four channel variants (E1371Q background). Data points represent mean ± SD from $n = 8$ (E1371Q), 6 (E92Q/E1371Q), 6 (S1141E/E1371Q), and 4 (E92Q/S1141E/E1371Q) patches and have been fitted as described under "Experimental procedures." *C*, mean K_D values for these channel variants obtained from such fits as a function of membrane potential. Data points represent mean ± SD from $n = 8$ (E1371Q), 6 (E92Q/E1371Q), 6 (S1141E/E1371Q), and 4 (E92Q/S1141E/E1371Q) patches. *D* and *E*, mean K_D values estimated at −40 mV (all E1371Q background). *D*, effect of E92Q on K_D in different E1371Q-containing channel backgrounds, as shown for conductance in Figure 5*D*. Data points represent mean ± SD from the same number of patches specified in (*E*). Whereas E92Q significantly increases K_D in a control, E1371Q background, it decreases K_D by >90% in K95Q/E1371Q, R134Q/E1371Q and S1141E/E1371Q backgrounds (see Results). *E*, K_D values for all channel variants studied (E1371Q background). Bars represent mean ± SD from $n = 8$ (E1371Q), 6 (E92Q/E1371Q), 6 (K95Q/E1371Q), 8 (R134Q/E1371Q), 4 (S1141E/E1371Q), 6 (S1141K/E1371Q), 5 (E92Q/K95Q/E1371Q), 4 (E92Q/R134Q/E1371Q), 6 (E92Q/S1141E/E1371Q), 4 (E92K/K95E/E1371Q), 5 (K95S/S1141K/E1371Q), and 8 (R134Q/S1141K/E1371Q) patches. Tests of significance were carried out using one-way ANOVA with Bonferroni correction. *Asterisks* indicate a significant difference from E1371Q (*$p < 0.05$; **$p < 0.001$). *Daggers* indicate a significant difference from the corresponding single pore mutant without E92Q (*i.e.*, K95Q/E1371Q, R134Q/E1371Q or S1141E/E1371Q) ($p < 0.001$). Data for K95Q/E1371Q and K95S/S1141K/E1371Q taken from (10); data for R134Q/E1371Q, S1141K/E1371Q and R134Q/S1141K/E1371Q taken from (11).

charged side chains at both the outer and inner mouths of the pore influence both anion binding (7, 9, 24, 25) and Cl^- conductance (5–9); in some cases, these fixed positive charges may also interact with nearby negative charges (26, 27). Whether these more distant regions of the pore also affect the localized charge balance within the inner vestibule remains to be investigated.

As described previously (10–15), removal of a positive charge from the inner vestibule (as in K95Q and R134Q) is highly disruptive to Cl^- conductance (Fig. 5) and

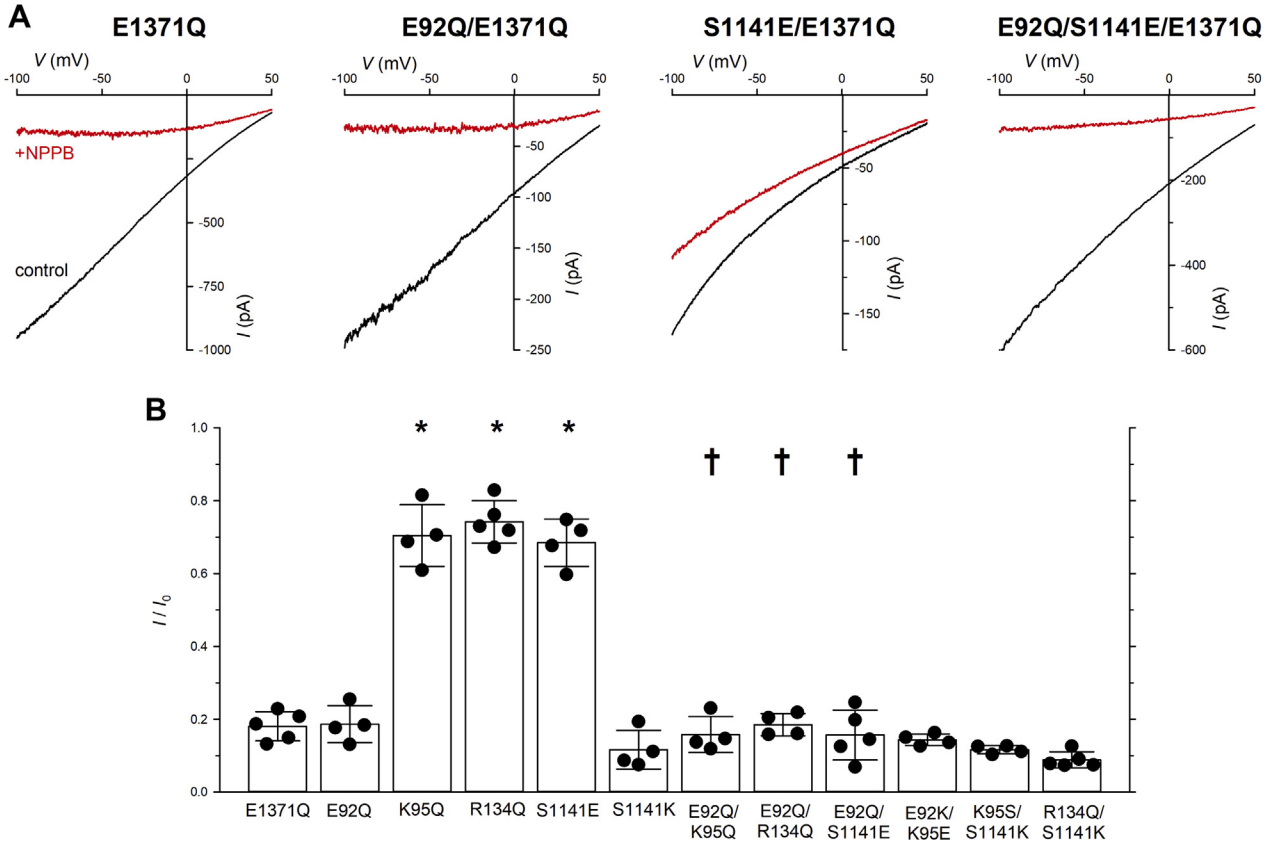

Figure 7. Block of Cl^- permeation by intracellular NPPB. *A*, example *I-V* relationships for the named variants, recorded before (*black lines*) and after addition of 50 μM NPPB to the intracellular solution (*red lines*). *B*, fraction of control current remaining after addition of this concentration of NPPB, at a membrane potential of −100 mV (all E1371Q background). Bars represent mean ± SD from n = 5 (E1371Q), 4 (E92Q/E1371Q), 4 (K95Q/E1371Q), 5 (R134Q/E1371Q), 4 (S1141E/E1371Q), 4 (S1141K/E1371Q), 4 (E92Q/K95Q/E1371Q), 4 (E92Q/R134Q/E1371Q), 5 (E92Q/S1141E/E1371Q), 4 (E92K/K95E/E1371Q), 4 (K95S/S1141K/E1371Q), and 5 (R134Q/S1141K/E1371Q) patches. Tests of significance were carried out using one-way ANOVA with Bonferroni correction. *Asterisks* indicate a significant difference from E1371Q ($p < 0.001$), while *daggers* indicate a significant difference from the corresponding single pore mutant without E92Q (*i.e.*, K95Q/E1371Q, R134Q/E1371Q, or S1141E/E1371Q) ($p < 0.001$). Data for R134Q/E1371Q, S1141K/E1371Q, and R134Q/S1141K/E1371Q taken from (11). NPPB, 5-nitro-2-(3-phenylpropylamino)benzoic acid.

anion-binding properties (Figs. 6–8). These effects were mimicked—and in some cases exceeded—by introducing an additional negative charge in the inner vestibule, in S1141E mutant channels. Thus, S1141E reduced Cl^- conductance below the limit of resolution (Fig. 5), drastically weakened block of Cl^- permeation by both $Au(CN)_2^-$ (Fig. 6) and NPPB (Fig. 7), and reversed Cl^-:SCN^- conductance selectivity (Fig. 8). It is perhaps not surprising that introducing a pore-lining negative charge should be disruptive to the function of an anion channel (although this is what nature has done in placing Glu^{92} close to an important anion-binding site in the CFTR pore). We hypothesize that the strong disruption of pore function observed in S1141E-mutant channels may reflect the important position of this amino acid close to an important anion-binding site involving Lys^{95} and Arg^{134} (Fig. 1), although we have not investigated the effects of introducing a negative charge at other sites in the inner vestibule. Importantly, all of the functional effects of S1141E can be "rescued" to some extent by the comutation E92Q (Figs. 5–8), and conversely, the strong block of E92Q/E1371Q by $S_2O_3^{2-}$ can be reversed by S1141E (Fig. 4). In effect, in E92Q/S1141E-mutant channels, a negative charge has been "transplanted" from TM1 to TM12 (Fig. 1), generally preserving pore conductance and anion-binding properties.

The nearby residues mutated in the present study—Glu^{92} (TM1), Lys^{95} (TM1), Arg^{134} (TM2), and Ser^{1141} (TM12) (Fig. 1)—contribute two fixed positive charges and one fixed negative charge to the inner vestibule of the pore. Mutations that decrease the "positivity" in this region—either by removing positive charges (K95Q, R134Q) or adding negative charge (S1141E)—drastically decrease conductance (by >90%) (Fig. 9*A*). Mutations that increase positivity—by adding positive charge (S1141K) or removing negative charge (E92N, E92Q, E92T)—have almost no effect on conductance (Fig. 9*A*). Mutations that retain the balance between positive and negative charge—either by conservative substitution (E92D), or by "moving" charges around different sites (E92Q/S1141E, E92K/K95E, K95S/S1141K, R134Q/S1141K), or by removing both negative and positive charges (E92Q/K95Q, E92Q/R134Q)—retain conductance (between 52 and 101% of wild-type conductance) (Fig. 9*A*), with the exception of E92Q/S1141E, which has a conductance 26 ± 2% of wild-type (n = 4); as discussed above, this may reflect the highly detrimental effects of having a negatively charged side chain at position 1141. We

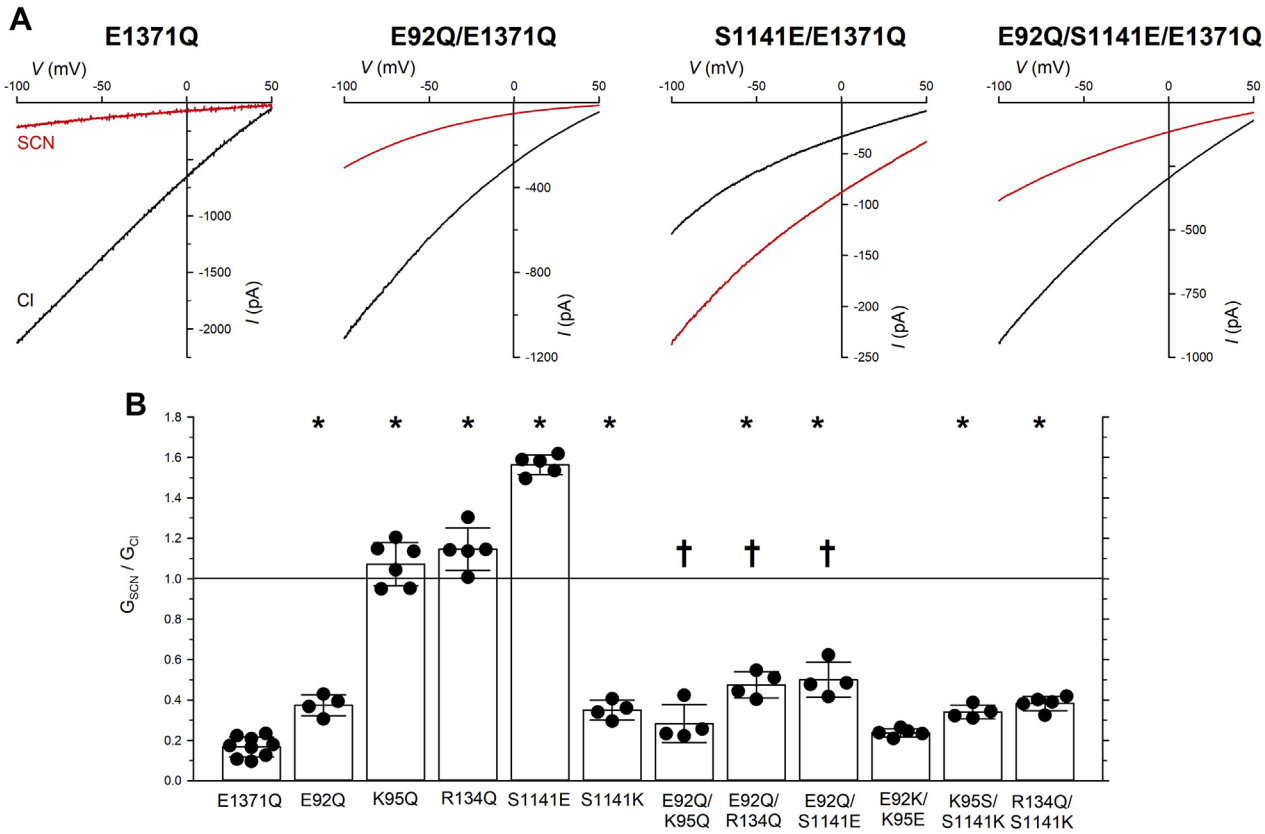

Figure 8. Relative SCN^- conductance of different channel variants. *A*, example *I-V* relationships for the named variants during perfusion with 154 mM Cl^- (*black lines*) or SCN^- (*red lines*) in the intracellular (bath) solution. *B*, relative SCN^- conductance (G_{SCN}/G_{Cl}) for different variants (E1371Q background), estimated from changes in the slope of macroscopic *I-V* relationships such as those shown in (*A*), as described under "Experimental procedures." Bars represent mean ± SD from $n = 9$ (E1371Q), 4 (E92Q/E1371Q), 6 (K95Q/E1371Q), 5 (R134Q/E1371Q), 5 (S1141E/E1371Q), 4 (S1141K/E1371Q), 4 (E92Q/K95Q/E1371Q), 4 (E92Q/R134Q/E1371Q), 4 (E92Q/S1141E/E1371Q), 5 (E92K/K95E/E1371Q), 4 (K95S/S1141K/E1371Q), and 5 (R134Q/S1141K/E1371Q) patches. Tests of significance were carried out using one-way ANOVA with Bonferroni correction. *Asterisks* indicate a significant difference from wild-type ($p < 0.001$). *Daggers* indicate a significant difference from the corresponding single pore mutant without E92Q (*i.e.*, K95Q/E1371Q, R134Q/E1371Q or S1141E/E1371Q) ($p < 0.001$). Data for K95Q/E1371Q taken from (15); data for R134Q/E1371Q, S1141K/E1371Q, and R134Q/S1141K/E1371Q taken from (11).

propose that it is the balance between positive and negative charges—rather than the number of charges—that controls conductance (Fig. 9*A*); an excess of positive charges is necessary for normal conductance, but increasing the excess from +1 to +2 causes little or no increase in conductance. Nevertheless, even for channels with one excess positive charge, there is a large variation of conductance (Fig. 9*A*). This may reflect that the exact position of the positive and negative charges within the inner vestibule has some influence on conductance; for instance, maximal conductance is obtained with positive charge at positions 95 and 134 and a negative charge at position 92 (wild-type, E92D), and other positions may be suboptimal "hosts" for these charges. Alternatively, unstudied factors other than charge may also be at play within the inner vestibule to modulate conductance.

Similarly to conductance, an excess of positive charge—achieved by any combination of positively and negatively charged side chains that has been investigated—is clearly required for high-affinity $Au(CN)_2^-$ binding (Fig. 9*B*), for NPPB block (Fig. 9*C*), and for Cl^-:SCN^- conductance selectivity (Fig. 9*D*). Since each of these parameters likely reflects aspects of anion binding in the inner vestibule (see the start of the text), it appears that an excess of positive charge is required to form a functional anion-binding site in the inner vestibule. Increasing the excess of positive charge (as in E92Q and S1141K) has practically no impact on these anion-binding parameters (or conductance, see above) (Fig. 9), but does lead to a drastic increase in the binding of the test divalent anion $S_2O_3^{2-}$ (Fig. 3; (19)). As discussed previously, strong binding of cytoplasmic divalent anions is likely to be detrimental to overall channel function (13, 19). The apparent lack of strong position dependence in the functional role of these charges is consistent with an electrostatic effect rather than, for example, structural changes due to charge-dependent interactions with other TMs.

Mutation of Glu^{92} also appears to have charge-dependent effects on the production of mature, complex-glycosylated CFTR protein (Fig. 2), suggesting that the presence of a negative charge at this position in important for CFTR protein folding and/or trafficking to the membrane. E92K is a CF-causing mutation (CFTR2 database, https://cftr2.org) that has previously been shown to have very low function and plasma membrane expression using other techniques (28). Mistrafficking of E92K was reversed by the comutation K95E,

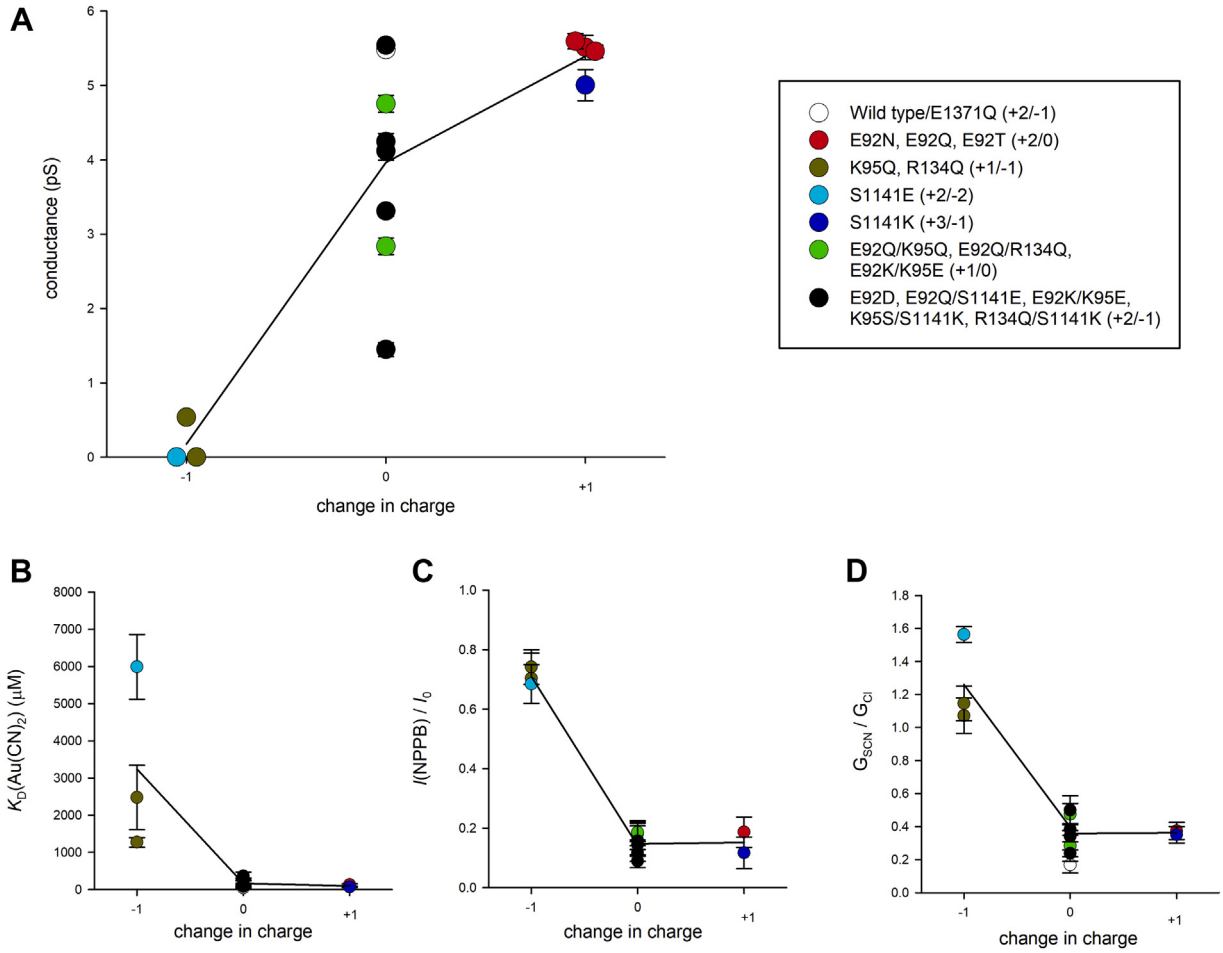

Figure 9. Effect of fixed charge in the inner vestibule on pore functional properties. *A*, conductance of different channel variants (taken from Fig. 5), as a function of the overall change in charge due to mutation. Different variants are grouped by color according to the number of positive and negative charges present at positions 92, 95, 134 and 1141, *e.g.*, wild-type (+2/−1), E92Q (+2/0), etc. (see legend). Note that for some mutants (S1141E, R134Q, E92N, E92T) the change in charge (*abscissa*) is slightly off-set for the sake of clarity; and that for S1141E and R134Q, conductance is below the limit of resolution. *B–D*, similar analysis of other pore properties (E1371Q background), *viz.*, (*B*) K_D for $Au(CN)_2^-$ at −40 mV (from Fig. 6), (*C*) NPPB block (Fig. 7), (*D*) G_{SCN}/G_{Cl} (Fig. 8). In all panels, data points represent mean ± SD from the number of patches specified in Figures 5–8.

which restores the overall balance of negative and positive side chains to TM1 (Fig. 2). While we have not studied the effect of mutations on CFTR protein processing in detail, one possibility is that this charge balance is important for the correct α-helical configuration of TM1 and/or its proper interaction with other TMs.

Our investigation is not the first example of an ion channel pore incorporating the "wrong" fixed charge in an ion-binding site. For example, voltage-gated Na^+ channels have both negative and positive charges surrounding their selectivity filters (the well-known "DEKA" locus); the positively charged lysine is thought to be important for high Na^+:K^+ selectivity (29–31). Among anion channels, ClCs have a conserved negatively charged glutamate side chain that can move to occupy a Cl^- binding site in the pore, which is thought to be important in permeation and gating in these channels (32, 33). However, in these examples, charged side chains make specific interactions with bound permeating ions, unlike the situation we describe in the CFTR pore, where it appears that the pore uses a combination of positive and negative charges to titrate the valence selectivity of a permeant ion-binding site. Is there any advantage to having an anion-binding site formed by a combination of two positive and one negative charges (as is apparently the case for wild-type CFTR), when a channel with one positive and no negative charges (such as E92Q/K95Q or E92Q/R134Q) is also able to sustain relatively high Cl^- conductance (Fig. 5)? We can only speculate that, since wild-type has a (slightly) higher conductance than other channel variants studied here (Fig. 5), this arrangement of positive and negative charges may be well suited for optimizing conductance without allowing detrimental strong binding of divalent anions (as is observed in E92N and E92Q). The wild-type pore also appears well optimized for tight binding of permeant anions (as quantified using $Au(CN)^-$ block) (Fig. 6), which has recently been proposed as being important in maximizing pore occupancy and thereby increasing conductance (10). Thus, the somewhat counterintuitive presence of a negatively charged side chain in an anion-binding site appears, in this case at least, to confer optimal anion binding and conductance properties to the channel.

Experimental procedures

Experiments were carried out on BHK cells transiently transfected with CFTR, as described previously (13). Additional mutations were introduced using the QuikChange site-directed mutagenesis system (Agilent Technologies) and verified by DNA sequencing. Mutations were introduced at four pore-lining sites that are predicted to be in close proximity in the inner vestibule of the pore—Glu^{92} (TM1), Lys^{95} (TM1), Arg^{134} (TM2), and Ser^{1141} (TM12) (Fig. 1). Previous work has suggested that the positive charges of both Lys^{95} and Arg^{134} can be "transplanted" to Ser^{1141} (by comutagenesis) with little disruption of pore function, leading to the suggestion that these neighboring residues are in functionally analogous positions in the pore (11, 13). All macroscopic current recordings (Figs. 3, 4 and 6–8) were carried out on very high open probability channels bearing the E1371Q mutation that effectively isolates effects on Cl^- permeation (10, 13, 15).

Western blotting for CFTR was carried out as described recently (11). Briefly, immunoblotting was performed on total cellular protein (5–30 μg, depending on the transfection) with monoclonal mouse anti-CFTR antibody (M3A7, Sigma-Aldrich) (1:2000 dilution) followed by secondary horseradish peroxidase-conjugated goat anti-mouse (Abcam Inc) (1:20,000 dilution). Relative expression of mature, complex glycosylated CFTR protein ("Band C", ∼175 kDa) and immature, core glycosylated protein ("Band B", ∼150 kDa) was assessed by densitometry analysis of scanned Western blot images using ImageJ (Version 1.48, National Institutes of Health).

Functional characterization of CFTR channels was carried out using single channel and macroscopic patch clamp recordings from inside-out membrane patches, as described in detail previously (13). For most experiments, the extracellular (pipette) solution contained (mM): 150 Na gluconate, 2 $MgCl_2$, 10 *N*-tris[hydroxymethyl]methyl-2-aminoethanesulfonate (TES), pH 7.4, and the intracellular (bath) solution contained (mM): 150 NaCl, 2 $MgCl_2$, 10 TES, pH 7.4, to generate an outwardly-directed $[Cl^-]$ gradient. To quantify the relative conductance of Cl^- and SCN^- ions (Fig. 8), the intracellular face of inside-out patches was perfused with the intracellular solution described above, or (mM): 154 NaSCN, 2 $Mg(OH)_2$, 10 TES, pH 7.4. In all experiments, activity of constitutively active E1371Q-containing channels was sustained using a low concentration of intracellular ATP (50 μM) to obviate ATP block (10, 13). Single channel activity was stimulated by exposure to protein kinase A catalytic subunit (PKA; 1–5 nM) plus 50 μM ATP in the intracellular solution. Current traces were filtered at 150 Hz (for macroscopic currents) or 50 Hz (for single channel currents) using an eight-pole Bessel filter, digitized at 1 kHz, and analyzed using pCLAMP10 software (Molecular Devices). Measurement of single channel and macroscopic current amplitudes and construction of leak-subtracted current–voltage (*I-V*) relationships were carried out as described previously (13). Membrane voltages were corrected for liquid junction potentials calculated using pCLAMP software.

Block of Cl^- permeation by intracellular $S_2O_3^{2-}$, $Au(CN)_2^-$, and NPPB was investigated by direct application of these substances to the intracellular face of inside-out patches from high-concentration stocks made up in normal intracellular solution, as described recently (10, 11, 19). For $S_2O_3^{2-}$ and $Au(CN)_2^-$, concentration–inhibition relationships were fitted by the equation:

$$\text{Fractional unblocked current} = 1 / (1 + ([B] / K_D)) \quad (1)$$

Where [B] is blocker ($S_2O_3^{2-}$ or $Au(CN)_2^-$) concentration, and K_D is the apparent blocker dissociation constant. Open-channel block of wild-type CFTR by $Au(CN)_2^-$ has a complex voltage dependence (10) (Fig. 6*C*), and the K_Ds of different variants are compared at −40 mV, the voltage at which block of wild-type is strongest (10) (Fig. 6*C*).

For $S_2O_3^{2-}$, the relationship between K_D and membrane potential (V) was fitted by the equation:

$$K_D(V) = K_D(0)\exp(-z\delta VF / RT) \quad (2)$$

where zδ is the measured effective valence of the blocking ion (actual valence (z) multiplied by the fraction of the transmembrane electric field apparently experienced during the blocking reaction (δ)), and F, R, and T have their usual thermodynamic meanings.

Relative conductance of SCN^- and Cl^- ions (G_{SCN}/G_{Cl}) was estimated by perfusion of the intracellular face of inside-out patches containing constitutively active E1371Q-CFTR channels with solutions containing high concentrations of these two anions (see above), as described previously (11, 15). Relative conductance was quantified by measuring the slope conductance of the relatively linear part of the current–voltage relationship between −100 and 0 mV.

Experiments were carried out at room temperature, 21 to 24 °C. Where shown, mean values are presented ±standard deviation (SD). For graphical presentation of mean values, error bars represent SD, and where no error bars are visible, SD is smaller than the size of the symbol. In some cases (Figs. 2*C*, 4*B*, 5*E*, 6*E*, 7*B* and 8*B*), individual data points are shown together with bars showing mean ± SD. Tests of significance were carried out using one-way ANOVA with Bonferroni correction, with $p < 0.05$ being considered statistically significant. Unless otherwise stated, chemicals were from Sigma-Aldrich except for $KAu(CN)_2$ (Strem Chemicals) and PKA (Promega).

Data availability

Original data generated or analyzed during this study are available from the corresponding author, Dr Paul Linsdell (paul.linsdell@dal.ca) upon reasonable request.

Supporting information—This article contains supporting information.

Author contributions—P. L. conceptualization; P. L. and C. L. I. formal analysis; P. L. and C. L. I. investigation; E. A. C. project administration; E. A. C. supervision; P. L. writing—original draft.

Funding and additional information—This work was supported by a grant from the Natural Sciences and Engineering Research Council of Canada (RGPIN/05124-2017) to P. L.

Conflict of interest—The authors declare that they have no conflicts of interest with the contents of this article.

Abbreviations—The abbreviations used are: BHK, baby hamster kidney; CF, cystic fibrosis; CFTR, cystic fibrosis transmembrane conductance regulator; MSD, membrane-spanning domain; NBD, nucleotide-binding domain; NPPB, 5-nitro-2-(3-phenylpropylamino)benzoic acid; PKA, protein kinase A catalytic subunit; TES, N-tris[hydroxymethyl]methyl-2-aminoethanesulfonate; TM, transmembrane α-helix.

References

1. Csanády, L., Vergani, P., and Gadsby, D. C. (2019) Structure, gating, and regulation of the CFTR anion channel. *Physiol. Rev.* **99**, 707–738
2. Linsdell, P. (2017) Architecture and functional properties of the CFTR channel pore. *Cell. Mol. Life Sci.* **74**, 67–83
3. Liu, F., Zhang, Z., Csanády, L., Gadsby, D. C., and Chen, J. (2017) Molecular structure of the human CFTR ion channel. *Cell* **169**, 85–95
4. Zhang, Z., Liu, F., and Chen, J. (2018) Molecular structure of the ATP-bound, phosphorylated human CFTR. *Proc. Natl. Acad. Sci. U. S. A.* **115**, 12757–12762
5. Smith, S. S., Liu, X., Zhang, Z.-R., Sun, F., Kriewall, T. E., McCarty, N. A., and Dawson, D. C. (2001) CFTR: Covalent and noncovalent modification suggests a role for fixed charges in anion conduction. *J. Gen. Physiol.* **118**, 407–431
6. Gong, X., and Linsdell, P. (2003) Molecular determinants and role of an anion binding site in the external mouth of the CFTR chloride channel pore. *J. Physiol.* **549**, 387–397
7. Zhou, J.-J., Fatehi, M., and Linsdell, P. (2008) Identification of positive charges situated at the outer mouth of the CFTR chloride channel pore. *Pflügers Arch.* **457**, 351–360
8. El Hiani, Y., and Linsdell, P. (2015) Functional architecture of the cytoplasmic entrance to the cystic fibrosis transmembrane conductance regulator chloride channel pore. *J. Biol. Chem.* **290**, 15855–15865
9. Li, M.-S., Cowley, E. A., El Hiani, Y., and Linsdell, P. (2018) Functional organization of cytoplasmic portals controlling access to the cystic fibrosis transmembrane conductance regulator (CFTR) chloride channel pore. *J. Biol. Chem.* **293**, 5649–5658
10. Linsdell, P. (2021) On the relationship between anion binding and chloride conductance in the CFTR anion channel. *Biochim. Biophys. Acta* **1863**, 183558
11. Linsdell, P., Irving, C. L., Cowley, E. A., and El Hiani, Y. (2021) Two positively charged amino acid side-chains in the inner vestibule of the CFTR channel pore play analogous roles in controlling anion binding and anion conductance. *Cell. Mol. Life Sci.* **78**, 5213–5223
12. Ge, N., Muise, C. N., Gong, X., and Linsdell, P. (2004) Direct comparison of the functional roles played by different transmembrane regions in the cystic fibrosis transmembrane conductance regulator chloride channel pore. *J. Biol. Chem.* **279**, 55283–55289
13. Zhou, J.-J., Li, M.-S., Qi, J., and Linsdell, P. (2010) Regulation of conductance by the number of fixed positive charges in the intracellular vestibule of the CFTR chloride channel pore. *J. Gen. Physiol.* **135**, 229–245
14. Linsdell, P. (2005) Location of a common inhibitor binding site in the cytoplasmic vestibule of the cystic fibrosis transmembrane conductance regulator chloride channel pore. *J. Biol. Chem.* **280**, 8945–8950
15. Linsdell, P. (2016) Anion conductance selectivity mechanism of the CFTR chloride channel. *Biochim. Biophys. Acta* **1858**, 740–747
16. Farkas, B., Tordai, H., Padányi, R., Tordai, A., Gera, J., Paragi, G., and Hegedűs, T. (2020) Discovering the chloride pathway in the CFTR channel. *Cell. Mol. Life Sci.* **77**, 765–778
17. El Hiani, Y., and Linsdell, P. (2012) Tuning of CFTR chloride channel function by location of positive charges within the pore. *Biophys. J.* **103**, 1719–1726
18. Linsdell, P. (2015) Interactions between permeant and blocking anions inside the CFTR chloride channel pore. *Biochim. Biophys. Acta* **1848**, 1573–1590
19. Linsdell, P. (2021) Monovalent: Divalent anion selectivity in the CFTR Channel Pore. *Cell Biochem. Biophys.* **79**, 863–871
20. Wang, W., El Hiani, Y., and Linsdell, P. (2011) Alignment of transmembrane regions in the cystic fibrosis transmembrane conductance regulator chloride channel pore. *J. Gen. Physiol.* **138**, 165–178
21. Gao, X., Bai, Y., and Hwang, T.-C. (2013) Cysteine scanning of CFTR's first transmembrane segment reveals its plausible roles in gating and permeation. *Biophys. J.* **104**, 786–797
22. Linsdell, P. (2014) State-dependent blocker interactions with the CFTR chloride channel: Implications for gating the pore. *Pflügers Arch.* **466**, 2243–2255
23. Fatehi, M., St Aubin, C. N., and Linsdell, P. (2007) On the origin of asymmetric interactions between permeant anions and the cystic fibrosis transmembrane conductance regulator chloride channel pore. *Biophys. J.* **92**, 1241–1253
24. St Aubin, C. N., Zhou, J.-J., and Linsdell, P. (2007) Identification of a second blocker binding site at the cytoplasmic mouth of the cystic fibrosis transmembrane conductance regulator chloride channel pore. *Mol. Pharmacol.* **71**, 1360–1368
25. Zhou, J.-J., Fatehi, M., and Linsdell, P. (2007) Direct and indirect effects of mutations at the outer mouth of the cystic fibrosis transmembrane conductance regulator chloride channel pore. *J. Membr. Biol.* **216**, 129–142
26. Rahman, K. S., Cui, G., Harvey, S. C., and McCarty, N. A. (2013) Modeling the conformational changes underlying channel opening in CFTR. *PLoS One* **8**, e74574
27. Wang, G., Linsley, R., and Norimatsu, Y. (2016) External Zn^{2+} binding to cysteine-substituted cystic fibrosis transmembrane conductance regulator constructs regulates channel gating and curcumin potentiation. *FEBS J.* **283**, 2458–2475
28. Prins, S., Langron, E., Hastings, C., Hill, E. J., Stefan, A. C., Griffin, L. D., and Vergani, P. (2020) Fluorescence assay for simultaneous quantification of CFTR ion-channel function and plasma membrane proximity. *J. Biol. Chem.* **295**, 16529–16544
29. Lipkind, G. M., and Fozzard, H. A. (2008) Voltage-gated Na channel selectivity: The role of the conserved domain III lysine residue. *J. Gen. Physiol.* **131**, 523–529
30. Li, Y., Liu, H., Xia, M., and Gong, H. (2016) Lysine and the Na^+/K^+ selectivity in mammalian voltage-gated sodium channels. *PLoS One* **11**, e0162413
31. Boiteaux, C., Flood, E., and Allen, T. W. (2018) Comparison of permeation mechanisms in sodium-selective ion channels. *Neurosci. Lett.* **700**, 3–8
32. Accardi, A. (2015) Structure and gating of CLC channels and exchangers. *J. Physiol.* **593**, 4129–4138
33. Jentsch, T. J., and Pusch, M. (2018) CLC chloride channels and transporters: Structure, function, physiology, and disease. *Physiol. Rev.* **98**, 1493–1590
34. Linsdell, P. (2018) Cystic fibrosis transmembrane conductance regulator (CFTR): Making an ion channel out of an active transporter structure. *Channels* **12**, 284–290